Lifetime Measurement of the 2_1^+ State in ^{20}C

M. Petri,[1,*] P. Fallon,[1] A. O. Macchiavelli,[1] S. Paschalis,[1] K. Starosta,[2,3,4] T. Baugher,[3,4] D. Bazin,[3] L. Cartegni,[5] R. M. Clark,[1] H. L. Crawford,[3,6] M. Cromaz,[1] A. Dewald,[7] A. Gade,[3,4] G. F. Grinyer,[3] S. Gros,[1] M. Hackstein,[7] H. B. Jeppesen,[1] I. Y. Lee,[1] S. McDaniel,[3,4] D. Miller,[3,4] M. M. Rajabali,[5] A. Ratkiewicz,[3,4] W. Rother,[7] P. Voss,[3,4] K. A. Walsh,[3,4] D. Weisshaar,[3] M. Wiedeking,[8] and B. A. Brown[4]

[1]*Nuclear Science Division, Lawrence Berkeley National Laboratory, Berkeley, California 94720, USA*
[2]*Department of Chemistry, Simon Fraser University, Burnaby, British Columbia, V5A 1S6, Canada*
[3]*National Superconducting Cyclotron Laboratory, Michigan State University, East Lansing, Michigan 48824, USA*
[4]*Department of Physics and Astronomy, Michigan State University, East Lansing, Michigan 48824, USA*
[5]*Department of Physics and Astronomy, University of Tennessee, Knoxville, Tennessee 37996, USA*
[6]*Department of Chemistry, Michigan State University, East Lansing, Michigan 48824, USA*
[7]*Institut für Kernphysik der Universität zu Köln, D-50937 Köln, Germany*
[8]*Lawrence Livermore National Laboratory, Livermore, California 94551, USA*

(Received 21 January 2011; published 30 August 2011)

Establishing how and when large N/Z values require modified or new theoretical tools is a major quest in nuclear physics. Here we report the first measurement of the lifetime of the 2_1^+ state in the near-dripline nucleus ^{20}C. The deduced value of $\tau_{2_1^+} = 9.8 \pm 2.8(\text{stat})^{+0.5}_{-1.1}(\text{syst})$ ps gives a reduced transition probability of $B(E2; 2_1^+ \rightarrow 0^+_{\text{g.s.}}) = 7.5^{+3.0}_{-1.7}(\text{stat})^{+1.0}_{-0.4}(\text{syst})$ e^2 fm^4 in good agreement with a shell model calculation using isospin-dependent effective charges.

DOI: 10.1103/PhysRevLett.107.102501 PACS numbers: 27.30.+t, 21.10.Tg, 23.20.Lv

The exotic combinations of neutrons (N) and protons (Z) found far from the region of beta stability can significantly affect nuclear structure and properties. Two effects currently receiving great theoretical and experimental interest are the changes in shell structure [1,2] and the physics of weakly bound neutrons, which may move outside the core for a sizable fraction of the time leading to spatially extended ''core-decoupled'' wave functions (e.g., neutron halo nuclei [3,4]). While changes in shell structure due to the valence nucleon-nucleon interaction have been successfully described within a shell model framework with well-bound states and using harmonic oscillator wave functions, the effects of weak binding and extended radial distributions go beyond such approaches and at some point the familiar models and assumptions will no longer be valid. Establishing how and when large N/Z values require modified or new theoretical tools is a major question in nuclear physics and is one that remains largely unanswered.

Neutron-rich carbon isotopes have attracted a great deal of attention recently with regards to the question of spatially extended and decoupled valence neutrons. For example, ^{19}C [5] and the dripline nucleus ^{22}C [6] are proposed to have ground-state neutron halo structures. Properties of excited states can also provide information on weak binding effects and over the past several years there have been a number of experiments measuring the electric quadrupole transition rate, $B(E2; 2_1^+ \rightarrow 0^+_{\text{g.s.}})$, in ^{16}C [7–9], ^{18}C [9] and ^{20}C [10]. These transition rates are among the lowest found throughout the nuclear chart and this fact has been cited by some (e.g., Refs. [9–12]) as evidence for a reduced coupling between the valence neutrons and the core nucleons. Indeed, the $B(E2)$ value recently reported for ^{20}C in Ref. [10] is far lower than expected from shell model calculations and was interpreted as evidence for a ''decoupling'' of valence neutrons from the core that goes beyond the usual shell model approach. Here, we present the first direct measure of the 2_1^+ state lifetime and $B(E2; 2_1^+ \rightarrow 0^+_{\text{g.s.}})$ transition strength in ^{20}C. The result is compared to data in neighboring nuclei and to predictions from a shell model calculation, and discussed in terms of the coupling between the valence neutrons and the core.

The experiment was performed at the National Superconducting Cyclotron Laboratory (NSCL) at Michigan State University. A ^{22}O secondary beam was produced by fragmenting a 140 MeV/nucleon primary ^{48}Ca beam on a 775 mg/cm^2 ^{9}Be production target. The A1900 separator [13] was used to select and transport the ^{22}O ions to the S800 beam line where they underwent reactions on a second 500 mg/cm^2 ^{9}Be target located at the target position of the S800 spectrograph [14], producing ^{20}C via the ^{9}Be(^{22}O, ^{20}C + γ)X two-proton knockout reaction. Incoming ^{22}O ions were identified on an event-by-event basis via their time-of-flight, while outgoing ^{20}C ions were identified by energy-loss and time-of-flight measurements. The ^{22}O beam rate was approximately 2×10^4 pps for 4 days with an energy of $\approx$ 101 MeV/nucleon and a 2.5% momentum dispersion.

Approximately 30% of the ^{20}C nuclei in this experiment were produced in the excited 2_1^+ state, located at an energy $\sim$1.6 MeV above the 0^+ ground state. Gamma decays from the $2_1^+ \rightarrow 0^+_{\text{g.s.}}$ transition were detected in SeGA [15], an array of 15 32-fold segmented high-purity germanium detectors, surrounding the S800 target position

and coupled to the new digital data acquisition system (DDAS) [16]. The detector segmentation defines the γ-ray emission angle and is used for event-by-event Doppler correction to the energy of the γ ray emitted from the fast moving nuclei ($v/c \sim 40\%$). SeGA was configured in two rings with seven detectors at 30° (Ring 1) and eight detectors at 140° (Ring 2) relative to the beam direction, and at a distance of 30.2 and 23.3 cm from the target, respectively. In this configuration SeGA had a full energy photo-peak efficiency of ~2% at 1 MeV for γ rays emitted in flight.

To determine the lifetime of the ^{20}C 2^+ state the recoil distance method (RDM) was applied using the Köln/NSCL plunger [17]; the RDM technique for fast beams and its implementation at the NSCL is described in Refs. [18–20]. A 3870 mg/cm^2 ^{184}W degrader foil was placed 0.1 mm downstream of the 500 mg/cm^2 ^{9}Be secondary reaction target. Gamma rays emitted before or after the degrader experience different Doppler shifts leading to different lab energies. By measuring the ratio of the number of γ rays at the two energies and knowing the time required to traverse the target-degrader gap it is possible to determine the lifetime of the γ-decaying state. The target and degrader thickness and their separation distance were chosen to maximize the ^{20}C production yield, and to be sensitive to a range for the ^{20}C 2_1^+ lifetime of 10–20 ps.

An event-by-event Doppler reconstructed spectrum of γ rays obtained from a sum of all germanium detectors and in coincidence with ^{20}C fragments is shown in the top panel of Fig. 1. The $2_1^+ \rightarrow 0_{\text{g.s.}}^+$ γ-ray transition is seen at 1618(6) keV, in good agreement with the previously measured values of 1588(20) [21], 1631(37), and 1614(11) keV [10]. Gamma-ray energies were Doppler corrected assuming the ^{20}C fragments are moving with a mean velocity of $v/c = 0.418$ corresponding to decays before the degrader. The mean velocity after the degrader is calculated to be $v/c \approx 0.350$. Gamma rays emitted at this lower velocity would be "overcorrected" and appear at ~1740 and ~1530 keV for detectors located at 140° and 30°, respectively. The spectrum in the top panel, with a single dominant peak, indicates the majority of the decays occur before the ^{20}C fragments have traversed the degrader.

The lower panels in Fig. 1 show γ-ray spectra separated according to detector angle. The left panel contains data (solid line histograms) from SeGA detectors located at 30°, the right panel from detectors at 140°. Superposed on the measured data are simulated spectra (dotted line) corresponding to a 2_1^+ state lifetime of $\tau = 10$ ps, for reference. The simulated spectra were obtained using a Monte Carlo based code, which models the incoming secondary beam properties, reaction kinematics, ion transport in matter, γ-ray detector response function, and momentum selection of the product fragments; details of this simulation code and analysis procedure are given in

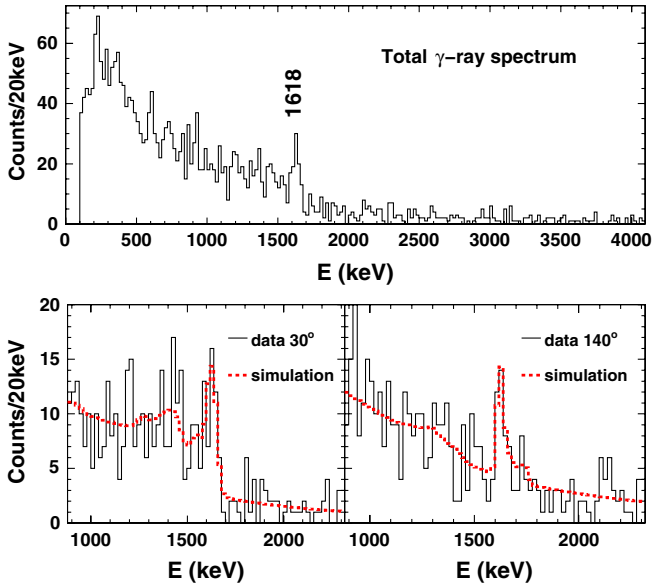

FIG. 1 (color online). Top panel: Spectrum of γ rays, after Doppler correcting with $v/c = 0.418$, obtained from a sum of all SeGA detectors and in coincidence with ^{20}C fragments. Lower panels: Spectra of γ rays for Ring 1 (30°) and Ring 2 (140°) after Doppler correcting with $v/c = 0.418$. Experimental data are shown as a black solid line. Simulated data for $\tau = 10$ ps are shown as a red dotted line.

Ref. [18]. A smooth background (given by an exponential plus constant term, $ae^{-bE_\gamma} + c$) was added to the Monte Carlo generated spectrum to account for the effects of beam induced bremsstrahlung and high energy γ rays not included in the Monte Carlo code. Simulated spectra (S_0), to be compared with the experimental one, were then given by $S_0 = ae^{-bE_\gamma} + c + n \times \text{MC}$, where MC is the output from the Monte Carlo code and n is a normalization factor. The variables (a, b, c, n) were obtained from a point estimation using the Poisson likelihood chi-square, $\chi^2_{\lambda,p}$, of Ref. [22] over the γ-ray energy range from 200 keV to 4 MeV. The lifetime (τ) was then extracted by minimizing $\chi^2_{\lambda,p}$ (noted hereafter as χ^2) with respect to τ over the spectrum region that includes the Doppler-shifted γ-ray peak components plus Compton edge. As seen in Fig. 2, a clear minimum in χ^2 as a function of the ^{20}C 2^+ lifetime is found at $\tau = 9.8 \pm 2.8$ ps. This lifetime value corresponds to an electric quadrupole transition rate of $B(E2; 2_1^+ \rightarrow 0_{\text{g.s.}}^+) = 7.5^{+3.0}_{-1.7}$ e^2 fm^4.

Reactions can also occur on the degrader, ^{184}W(^{22}O, ^{20}C + γ)X, producing "contaminant" ^{20}C γ rays that can add to the "slow" peak component. The ratio of target to degrader reactions producing ^{20}C was estimated to be $1.8^{+0.5}_{-0.4}$, by normalizing it to the ratio of reactions in the target and degrader measured in a similar experiment with ^{16}C [23]. This effect was included in the simulation code. The uncertainty due to reactions on the ^{184}W degrader foil adds a

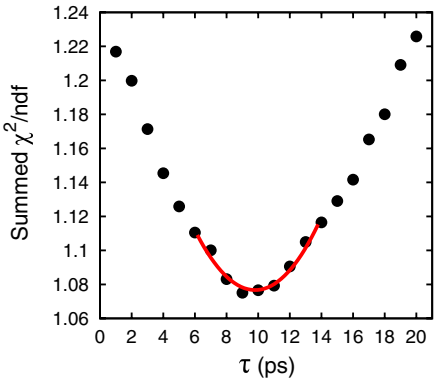

FIG. 2 (color online). χ^2 minimization for the lifetime of the ^{20}C 2_1^+ state. The y axis is the sum χ^2 normalized to the number of degrees of freedom (ndf) obtained from fits to the 30° and 140° γ-ray spectra. The red solid line is a parabolic fit to a lifetime range of 6–14 ps, which defines the minimum χ^2 at a lifetime of $\tau_{2_1^+} = 9.8 \pm 2.8$ ps.

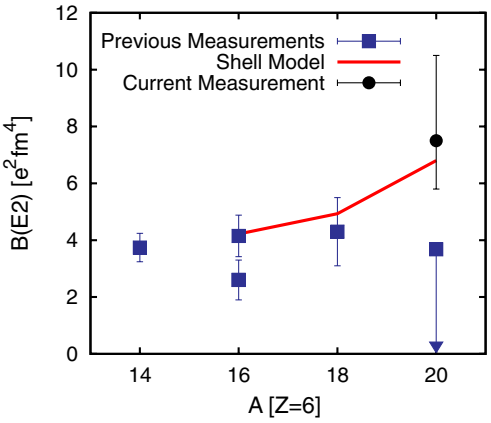

FIG. 3 (color online). $B(E2; 2_1^+ \rightarrow 0^+_{\text{g.s.}})$ trend in even mass carbon isotopes for $A = 16$–20 including only statistical errors. Previous data include ^{14}C [34], ^{16}C [8,9], ^{18}C [9], ^{20}C [10]. We note that $B(E2)$ values for ^{16}C [23] and ^{18}C [35] obtained at the NSCL using the same RDM technique as the current ^{20}C measurement agree well with the ^{16}C and ^{18}C $B(E2)$ values plotted here. The red solid line is a shell model calculation discussed in the text.

systematic error, $\tau_{2_1^+} = 9.8 \pm 2.8(\text{stat})^{+0.5}_{-1.1}(\text{syst})$ ps and $B(E2; 2_1^+ \rightarrow 0^+_{\text{g.s.}}) = 7.5^{+3.0}_{-1.7}(\text{stat})^{+1.0}_{-0.4}(\text{syst})$ e^2 fm^4.

We will now discuss the lifetime and $B(E2)$ result in the context of weak binding and the potential decoupling of valence neutrons from the core. For $N > 8$ the valence neutrons in carbon isotopes occupy the *sd* shell and (in carbon) the $d_{5/2}$ and $s_{1/2}$ orbits are near degenerate [21]. The four valence protons fill the $p_{3/2}$ level and, because the separation between the $p_{3/2}$ and $p_{1/2}$ levels at $Z = 6$ is large (several MeV) [24], the 2_1^+ excitation has a dominant neutron character associated with transitions within the neutron *sd* shell. The occupancy (spectroscopic factors) of neutrons in the *sd* shell was recently measured for ^{16}C [25] showing a significant neutron configuration mixing and $s_{1/2}$ amplitude in the lowest 2^+ and 0^+ states. (Occupation of the $s_{1/2}$ orbital leads to the halo structures reported in the weakly bound ^{19,22}C and the anomalous $B(M1)$ transition strength in ^{17}C [26,27].) Since only protons directly contribute to the electric quadrupole transition strength, a measure of the $B(E2; 2_1^+ \rightarrow 0^+_{\text{g.s.}})$ can, in cases where the lowest lying 2^+ state has a predominant neutron excitation, provide information on the coupling between the valence neutrons and the core protons due to core polarization. Core polarization effects decrease when the binding energy of the valence nucleons becomes small, as these nucleons spend less time near the core, (see the example of ^{209}Pb, Ref. [28]) and the observation of a suppressed electric transition rate can therefore be a signature for weakly bound and decoupled neutrons.

Experimental $B(E2; 2_1^+ \rightarrow 0^+_{\text{g.s.}})$ values are shown in Fig. 3 for even mass carbon isotopes with $A = 14$–20. The data indicate a rather constant, possibly slightly increasing trend in $B(E2; 2_1^+ \rightarrow 0^+_{\text{g.s.}})$ for ^{14,16,18}C in the range of 3–4 e^2 fm^4. The $B(E2)$ value for ^{20}C obtained in this work shows this trend continuing and even to increase further. This is in marked contrast to the decreasing $B(E2)$ suggested by Ref. [10], i.e., ^{20}C $B(E2; 2_1^+ \rightarrow 0^+_{\text{g.s.}}) < 3.68$ e^2 fm^4, which was derived indirectly from an inelastic scattering measurement. The significance in the difference between the two results for ^{20}C becomes apparent when comparing with theory (solid line in Fig. 3), which predicts a relatively high value for the ^{20}C $B(E2)$ consistent with the result reported here. The calculated transition rates (Table I) are given by $B(E2; J_i \rightarrow J_f) = |A_p e_p + A_n e_n|^2/(2J_i + 1)$, where A_p and A_n are shell model proton and neutron quadrupole matrix elements connecting the $J_i = 2_1^+$ and $J_f = 0^+_{\text{g.s.}}$ states calculated in a *p-sd* shell model space using harmonic oscillator wave functions and the WBT interaction [29], and e_p, e_n are the effective charges for protons and neutrons from Ref. [30]. We note that other variants of the interaction in the *p-sd* model space such as WBP [29] and WBT* [21] give ^{20}C $B(E2)$ values of 6.39 and 7.58 e^2 fm^4, respectively, using the effective charges of Table I. Similar changes are seen for ^{16}C and ^{18}C, and can be used to judge the theoretical error within the context of the *p-sd* model space. However, as shown in Fig. 13 of Ref. [9] other

TABLE I. Calculated $B(E2)$ values for ^{16,18,20}C. A_p and A_n are proton and neutron quadrupole matrix elements calculated in a *p-sd* shell model space using the WBT interaction [29], e_p and e_n are effective charges from Ref. [30].

	A_p	A_n	e_p	e_n	$B(E2)$(e^2 fm^4)
^{16}C	1.28	9.39	1.16	0.33	4.22
^{18}C	1.76	11.16	1.11	0.27	4.93
^{20}C	3.06	11.48	1.07	0.22	6.80

calculations, e.g., AMD, deformed Skyrme Hartree-Fock and the "no-core" shell model, can give very different $B(E2)$ values.

Effective charges [31], within a given model space, carry information on the degree of core polarization induced by the valence neutrons, and their magnitude (*suppression*) can then be a measure of the neutron-core (*de*)coupling. Effective charges are generally not expected to be constant as a function of increasing asymmetry $(N - Z)$, but to have an approximate $1/A$ dependence [32]. In Table I the e_p and e_n values are taken from the calculation in Ref. [30] based on the treatment in Ref. [32], and follow $\sim 1/A$. Taking these effective charges to be the appropriate reference (for "normally" coupled neutrons), the agreement between our measured ^{20}C $B(E2)$ value and calculation indicates that the current shell model using well-bound wave functions contains the relevant physics to describe these data and the ^{20}C valence neutrons do not exhibit additional weak binding effects. ^{20}C with a calculated binding energy of about 4.5 MeV is not a candidate for a halo nucleus.

Why does the ^{20}C $B(E2; 2_1^+ \rightarrow 0_{\text{g.s.}}^+)$ increase? In the shell model, the attractive interaction between the $\nu d_{5/2} - \pi p_{1/2}$ orbits and repulsion between the $\nu d_{5/2} - \pi p_{3/2}$ orbits means that as neutrons fill the $d_{5/2}$ level there is a decrease in the proton $p_{3/2} - p_{1/2}$ separation (see, for example, Refs. [26,33]), which favors more "in-shell" $(p_{3/2} - p_{1/2})$ proton excitations. It is this increase in the proton admixture to the 2_1^+ that leads to a larger $B(E2)$ in ^{20}C compared with ^{16,18}C. This effect is not seen in oxygen isotopes since the $p_{1/2}$ state is full; $B(E2)$ values for oxygen are shown and discussed in Fig. 3 of Ref. [10]. The increase in A_p for $A = 20$ reflects the increase in proton excitations contributing to the ^{20}C 2_1^+ state. Considering the ^{20}C 2_1^+ state to be $|2^+\rangle = \alpha|\nu(sd)^6\rangle + \beta|\pi(p)^{-2}\rangle$, the shell model spectroscopic factors give $\beta \approx 0.5$. It is thus a highly mixed state with large components from both neutrons and protons, in contrast to the initial premise of decoupled motion. For ^{16}C and ^{18}C a similar analysis gives $\beta \approx 0.2$ and 0.3, respectively, consistent with the picture of increasing proton contribution to the 2^+ state of the neutron-rich carbon isotopes as a function of the neutron number.

To conclude, we have reported the first direct measurement of the lifetime and electric quadrupole transition strength $B(E2; 2_1^+ \rightarrow 0_{\text{g.s.}}^+)$ of the ^{20}C 2_1^+ state, and compared this value to those in neighboring isotopes and to a shell model calculation with effective charges that follow an approximate $1/A$ dependence. No evidence was found for dramatic changes in the behavior of the $B(E2)$ across the $N = 10,12,14$ carbon chain up to ^{20}C, in contrast to Ref. [10]. The motivation for this work was to test the applicability of current theories in regions of large N/Z values and help guide future experimental studies on nuclei close to the driplines. The new data lead to the important result that the shell model calculation used here (with well-bound wave functions) can provide a quantitative description of the $B(E2)$ transition rates in these carbon isotopes to within two neutrons of the dripline located at ^{22}C.

This work is supported in part by the Department of Energy, Office of Nuclear Physics under contracts No. DE-AC0205CH11231 and No. DE-AC52-07NA27344, and by the National Science Foundation under grants PHY-0606007 and PHY-0758099.

*MPetri@lbl.gov

[1] O. Sorlin and M.-G. Porquet, Prog. Part. Nucl. Phys. **61**, 602 (2008).
[2] T. Otsuka *et al.*, Phys. Rev. Lett. **95**, 232502 (2005).
[3] I. Tanihata *et al.*, Phys. Rev. Lett. **55**, 2676 (1985).
[4] P. G. Hansen and B. Jonson, Europhys. Lett. **4**, 409 (1987).
[5] A. Ozawa *et al.*, Nucl. Phys. **A691**, 599 (2001).
[6] K. Tanaka *et al.*, Phys. Rev. Lett. **104**, 062701 (2010).
[7] N. Imai *et al.*, Phys. Rev. Lett. **92**, 062501 (2004).
[8] M.Wiedeking *et al.*, Phys. Rev. Lett. **100**, 152501 (2008).
[9] H. J. Ong *et al.*, Phys. Rev. C **78**, 014308 (2008).
[10] Z. Elekes *et al.*, Phys. Rev. C **79**, 011302(R) (2009).
[11] Z. Elekes *et al.*, Phys. Lett. B **586**, 34 (2004).
[12] H. J. Ong *et al.*, Phys. Rev. C **73**, 024610 (2006).
[13] D. J. Morrissey *et al.*, Nucl. Instrum. Methods Phys. Res., Sect. B **204**, 90 (2003).
[14] D. Bazin *et al.*, Nucl. Instrum. Methods Phys. Res., Sect. B **204**, 629 (2003).
[15] W. F. Mueller *et al.*, Nucl. Instrum. Methods Phys. Res., Sect. A **466**, 492 (2001).
[16] K. Starosta *et al.*, Nucl. Instrum. Methods Phys. Res., Sect. A **610**, 700 (2009).
[17] A. Dewald *et al.*, GSI Sci. Rep. **2005**, 38 (2006).
[18] P. Adrich *et al.*, Nucl. Instrum. Methods Phys. Res., Sect. A **598**, 454 (2009).
[19] K. Starosta *et al.*, Phys. Rev. Lett. **99**, 042503 (2007).
[20] A. Dewald *et al.*, Phys. Rev. C **78**, 051302R (2008).
[21] M. Stanoiu *et al.*, Phys. Rev. C **78**, 034315 (2008).
[22] S. Baker and R. D. Cousins, Nucl. Instrum. Methods Phys. Res. **221**, 437 (1984).
[23] M. Petri *et al.* (to be published).
[24] M. A. Firestone *et al.*, Nucl. Phys. **A258**, 317 (1976).
[25] A. H. Wuosmaa *et al.*, Phys. Rev. Lett. **105**, 132501 (2010).
[26] T. Suzuki and T. Otsuka, Phys. Rev. C **78**, 061301(R) (2008).
[27] D. Suzuki *et al.*, Phys. Lett. B **666**, 222 (2008).
[28] A. Bohr and B. R. Mottelson, *Nuclear Structure* (W. A. Benjamin, Massachusetts, 1975), Vol. 1, p. 335.
[29] E. K. Warburton and B. A. Brown, Phys. Rev. C **46**, 923 (1992).
[30] H. Sagawa *et al.*, Phys. Rev. C **70**, 054316 (2004).
[31] B. A. Brown, A. Arima, and J. B. McGrory, Nucl. Phys. **A277**, 77 (1977).
[32] A. Bohr and B. R. Mottelson, *Nuclear Structure* (W. A. Benjamin, Massachusetts, 1975), Vol. 2, p. 514.
[33] P. Federman, S. Pittel, and A. Etchegoyen, Phys. Lett. B **140**, 269 (1984).
[34] S. Raman *et al.*, Atom. Data Nucl. Data **36**, 1 (1987).
[35] P. Voss *et al.* (to be published).